

Article

Effects of Nb and W Additions on the Microstructures and Mechanical Properties of Novel γ/γ' Co-V-Ti-Based Superalloys

Xingjun Liu ^{1,2}, Yunwei Pan ¹, Yuechao Chen ¹, Jiajia Han ¹ , Shuiyuan Yang ¹, Jingjing Ruan ¹, Cuiping Wang ^{1,*}, Yuansheng Yang ³ and Yingju Li ³

¹ Department of Materials Science and Engineering, College of Materials and Fujian Provincial Key Laboratory of Materials Genome, Xiamen University, Xiamen 361005, China; lxj@xmu.edu.cn (X.L.); ywpan@stu.xmu.edu.cn (Y.P.); cycfoxmu@foxmail.com (Y.C.); jiajiahan@xmu.edu.cn (J.H.); yangshuiyuan@xmu.edu.cn (S.Y.); ruanjingjingtohoku@163.com (J.R.)

² Department of Materials Science and Engineering, Harbin Institute of Technology, Shenzhen 518055, China

³ Institute of Metal Research, Chinese Academy of Sciences (CAS), Shenyang 110016, China; ysyang@imr.ac.cn (Y.Y.); yjli@imr.ac.cn (Y.L.)

* Correspondence: wangcp@xmu.edu.cn; Tel.: +86-592-2180606

Received: 14 June 2018; Accepted: 16 July 2018; Published: 23 July 2018



Abstract: Microstructures, elemental partition behavior, phase stabilities and mechanical properties of Nb- and W-containing Co-V-Ti-based superalloys were investigated. Elemental partition coefficients ($K_X = C_{\gamma'}/C_{\gamma}$) of Nb and W in Co-V-Ti-based superalloys are 2.07 and 1.10, respectively. The γ' solvus temperatures are determined as 1023 °C, 1055 °C and 1035 °C in Co-12V-4Ti, Co-10V-4Ti-2Nb and Co-10V-4Ti-2W alloys, which are higher than those of Co-9Al-9W alloy (1000 °C). The mass densities of quaternary Co-10V-4Ti-2Nb and Co-10V-4Ti-2W alloys are about 8.31 and 8.50 g·cm⁻³, respectively, which are 15% lower than Co-Al-W-based superalloys (9.8 g·cm⁻³). All examined alloys exhibit an anomalous positive dependence on temperature rising from 600 to 750 °C. Strengths of all examined alloys are higher than those of MarM509 (traditional Cobalt-based superalloy) and Co-9Al-9W at all temperatures that we investigated. The maximum flow stress of Co-V-Ti-Nb alloy is about 638 MPa at 750 °C while that of Co-V-Ti-W alloy is about 588 MPa at 700 °C.

Keywords: Cobalt-based superalloys; gamma prime; microstructure evolution; high-temperature mechanical properties

1. Introduction

Superalloys are widely used in fabricating critical parts in gas turbines of power plants, aircraft engines and chemical process industries, where the current operating temperatures have reached 1600 °C [1–5]. The ability to withstand load at operating temperatures close to their melting points is an important performance requirement for high temperature materials. Nickel-based superalloys strengthened by γ' (L1₂)-precipitates phase are the most commercially successful among all classes [3,6]. The operating temperatures of Nickel-based superalloys have exceeded 80% of their incipient melting temperatures, fractions that are higher than any other class of engineering alloys. Cobalt-based superalloys are often considered as possible alternatives to Nickel-based superalloys whose solidus and liquidus are 50–150 °C lower than the former [7]. In addition, all common alloying elements for superalloys have lower diffusion coefficients and lower stacking fault energies in cobalt than in nickel [8].

The ordered γ' (L1₂)-precipitates phase was reported in Cobalt-based alloys for the first time in 1971 [9]. Subsequently, Sato et al. reported new γ' phase Co₃(Al, W) in 2006 [7], which has accelerated

the researchs of Cobalt-based superalloys and renewed the worldwide scientific interest [10–13]. Currently, several γ' (L_{12})-precipitates in Cobalt-based alloys, such as tungsten containing $\text{Co}_3(\text{Ge}, \text{W})$ [14] and $\text{Co}_3(\text{Ga}, \text{W})$ [15], have been discovered and effects of alloying elements B, V, Ti, Cr, Mn, Fe, Ni, Nb, Mo, Ta, Re and Hf in novel Cobalt-based superalloys have also been investigated [7,16–23]. At present, the investigations on Cobalt-based superalloys mainly imitate the previous research on Nickel-based superalloys. Previous studies on high temperature creep properties (both single crystals [24–26] and poly crystals [20,27–29]) and flow stress behavior [16,17,20] for several Cobalt-based superalloys have been reported. More importantly, the dislocation behavior and stacking-fault formation during plastic deformation of Cobalt-based superalloys have also been reported [26,28,30,31]. The partition coefficients of alloying elements have been measured in quaternary and some quinary alloys [32–35], which have strong impacts on mechanical properties, microstructures and lattice parameter misfits. The positive lattice-parameter misfits in Cobalt-based superalloys cause γ' (L_{12})-precipitate rafting along $\langle 100 \rangle$ -type directions to occur parallel to the tensile loading and perpendicular to the compressive loading directions, which indicate that Cobalt-based superalloys might have good high-temperature creep properties [36].

Even if Cobalt-based superalloys have such great potential, Co-Al-W-based alloys possess high mass densities due to requirement of high tungsten content (7–10%) for stabilizing γ' (L_{12})-precipitates [37]. The mass densities of Nickel-based superalloys are between 8.2 and $9.3 \text{ g}\cdot\text{cm}^{-3}$, while Co-Al-W-based superalloys can reach up to $9.8 \text{ g}\cdot\text{cm}^{-3}$ [2,9,38,39]. Because of high densities, Co-Al-W-based alloys are inappropriate for applications such as turbine blades for aircraft engines where the strength to weight ratio is important. Recently, Makineni et al. discovered new tungsten free Co-Al-Mo-Nb/Ta-based superalloys strengthened by γ' - $\text{Co}_3(\text{Al}, \text{Mo}, \text{Nb}/\text{Ta})$ with mass densities in the range of 8.1 – 8.6 gm^{-3} and higher specific strengths [38]. However, in both tungsten free Co-Al-Mo-Nb/Ta and Co-Al-W-based alloys, the γ' precipitates are metastable and decompose at high temperature [38,40]. A stable tungsten-free γ' (L_{12})-precipitates phase Co_3Ti exists in the binary Co-Ti system [9], which shows the highest temperature of maximum flow stress among all the intermetallics with ordered L_{12} structure [41]. Zenk et al. have developed Co-11Ti-15Cr superalloy with a low density ($8.1 \text{ g}\cdot\text{cm}^{-3}$), which shows a maximum flow stress of about 590 MPa at $800 \text{ }^\circ\text{C}$ [42]. Development of novel Cobalt-based superalloys strengthened by γ' - Co_3Ti phase might be a breakthrough point of high temperature materials.

Our previous study has confirmed the existence of γ' (L_{12})-precipitates $\text{Co}_3(\text{V}, \text{Ti})$ phase in ternary Co-V-Ti system. Addition of V has significantly decreased the γ/γ' lattice parameter misfit of γ' (L_{12})-precipitates phase Co_3Ti and V is also proven to increase the γ' (L_{12})-solvus temperatures of the alloys containing γ' - Co_3Ti [43]. The maximum flow stress of γ' - Co_3Ti has been confirmed to be increased with the addition of V, and Co-Ti-V ternary alloy also shows the attractive strength [44]. More importantly, γ/γ' two-phase Co-V-Ti-Al and Co-V-Ti-Ni alloys have been reported. Co-V-Ti-Al alloy shows a maximum flow stress of about 355 MPa at $700 \text{ }^\circ\text{C}$ and Co-V-Ti-Ni alloy shows a maximum flow stress of about 544 MPa at $750 \text{ }^\circ\text{C}$ [45]. Although Co-V-Ti-based superalloys have such great mechanical properties, their strengths are still much lower than the Nickel-based superalloys. The further studies in Co-V-Ti-based superalloys are required and the γ/γ' two-phase Co-V-Ti-based alloys might be helpful in further reducing mass densities of superalloys.

Nb and W have been confirmed to be strong γ' -former elements in γ' -strengthened Cobalt-based superalloys [13,34,46]. The addition of Nb can improve the stabilities of γ' and increase the volume fractions of γ' (L_{12})-precipitates in several superalloys. The elemental partition coefficients of Nb approach 3 in several Co-Al-W-based superalloys [13]. Nb addition also leads to stabilize the γ' phase in Co-Al-Mo alloys [38]. W has been proven to be an important part of Cobalt-based superalloys strengthened by γ' (L_{12})-precipitates. The increase of W in Co-Al-W ternary system causes significant augment of γ' (L_{12})-precipitate volume fraction where increasing W from 8 to 11 at. % leads to a rise in volume fraction from 34% to 73% [47]. The increase in W also leads to an increase in γ' (L_{12})-solvus temperature from $840 \text{ }^\circ\text{C}$ to $1100 \text{ }^\circ\text{C}$ [34,46,47].

In this study, quaternary γ/γ' two-phase Co-V-Ti-X (X: Nb, W) were prepared. The influence of alloying elements Nb and W to Co-V-Ti-based alloys on microstructures, elemental partition behavior, phase stabilities and mechanical properties were investigated.

2. Materials and Methods

According to our previous study [43], the γ -(α Co) + γ' -Co₃Ti phase equilibrium at 800 °C (solid lines) and 1100 °C (dotted lines) are shown in Figure 1. To obtain the γ/γ' two-phase Co-V-Ti ternary alloy, the Co-V-Ti ternary master alloy has a composition of Co-12V-4Ti (at. %). The γ/γ' two-phase Co-10V-4Ti-2X (X: Nb, W) alloys have also been prepared in this study to investigate effects of Nb and W additions on the microstructures and mechanical properties of Co-V-Ti-based superalloys. A laboratory-scale vacuum arc melting furnace was used to melt alloys under Ar back-filled atmosphere for at least 10 times to improve composition homogeneity. The purities of raw elements used in this study exceeded 99.9%. The Co-12V-4Ti, Co-10V-4Ti-2Nb and Co-10V-4Ti-2W alloys are designated as CVT-1, CVTN and CVTW, respectively. The designations and compositions of these alloys which are measured by electron probe microanalyser (JXA-8100, JEOL, Tokyo, Japan) are shown in Table 1. The samples for microstructure observations and compressive tests are polycrystalline. The cast rods were solutionized at 1200 °C for 2.5 h and aged at 800 °C for 100 h under vacuum (10^{-5} mbar) in a vertical furnace followed by water quenching.

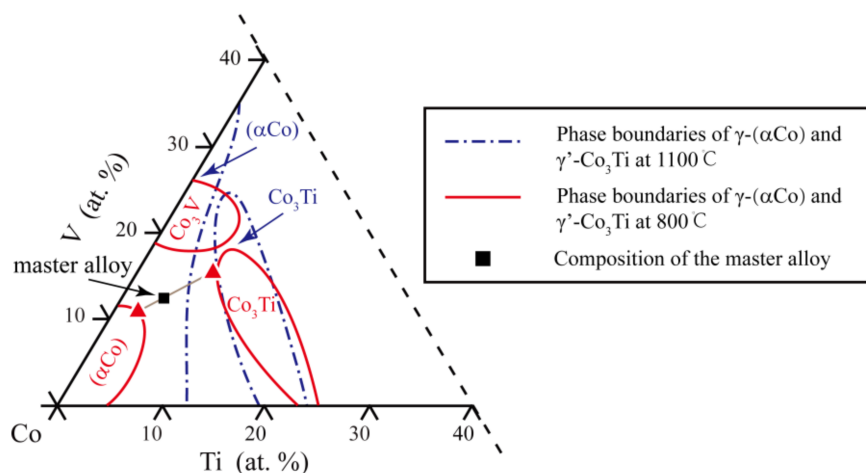


Figure 1. Phase equilibria in the Co-rich corner of the Co-Ti-V ternary system at 800 and 1100 °C (data from [43]).

Table 1. Nominal and measured composition of alloys in present investigation.

Alloy Designation	Nominal Composition (at. %)	Measured Composition (at. %)
CVT-1	Co-12V-4Ti	Co-(12.1 ± 0.2)V-(4.2 ± 0.1)Ti
CVTN	Co-10V-4Ti-2Nb	Co-(10.1 ± 0.1)V-(4.1 ± 0.2)Ti-(2.2 ± 0.2)Nb
CVTW	Co-10V-4Ti-2W	Co-(9.9 ± 0.2)V-(4.1 ± 0.2)Ti-(2.1 ± 0.1)W

The investigations of microstructures were carried out by a field emission scanning electron microscope with a secondary electron detector (SU-70, Hitachi, Ibaraki, Japan) at 10 kV acceleration voltage. The samples for SEM were mechanically polished, and then etched in a solution of HNO₃ (vol. 60%) + HCl (vol. 20%) + H₂O (vol. 20%) for a few seconds. The crystal structures of the γ/γ' phases and semiquantitative analyses of the partition behavior between γ/γ' interfaces were obtained by using a transmission electron microscope equipped with field emission source (F200 model, FEI, Hillsboro, OR, USA). Twin jet electropolishing at −30 °C and 18–20 V in a solution of HClO₄ (vol. 8%) + CH₃COOH (vol. 72%) + CH₃CH₂OH (vol. 12%) + HOCH₂CH₂OH (vol. 8%) was used to prepared

the foil specimens for TEM analyses. The volume fractions of γ' in the heat-treated samples were measured by using the manual point count method on several microstructure images recorded near a $\{100\}$ -type plane. The multiple results were averaged to approximate the actual volume fractions of γ' precipitates.

Differential scanning calorimetry (DSC) under an argon atmosphere, performed by NETZSCH DSC 404 (NETZSCH, Selb, German), was used to determine the phase transformation temperatures of heat treated alloys. Heating and cooling rates were $10\text{ }^\circ\text{C}\cdot\text{min}^{-1}$ in this study. The characteristic phase transition temperatures were determined by peak analysis of DSC curves.

The investigated mechanical properties comprised hardness and 0.2% flow stress. The hardness values of samples were measured by using Vickers micro hardness tester (HMV-2, Shimadzu, Kyoto, Japan) with a load of 9.8 N. The 0.2% flow stresses were determined from compressive tests at $25\text{ }^\circ\text{C}$, $600\text{ }^\circ\text{C}$, $700\text{ }^\circ\text{C}$, $750\text{ }^\circ\text{C}$, $800\text{ }^\circ\text{C}$, $900\text{ }^\circ\text{C}$, and $1000\text{ }^\circ\text{C}$ and the strain rate is $1 \times 10^{-4}\text{ s}^{-1}$. The samples for compressive tests were cut into the shape with dimension of $\phi 6\text{ mm} \times 9\text{ mm}$ by wire-cutting machine, and surfaces of the specimens were slightly polished.

3. Results and Discussions

3.1. Microstructure Evolution

Figure 2a–c presents the dark-field TEM images (DFI) and selected area diffraction patterns (SADP) obtained from CVT-1, CVTN and CVTW alloys aged at $800\text{ }^\circ\text{C}$ for 100 h. The diffraction patterns along $[001]$ zone axis contain superlattice reflections along with the main fcc reflections for both the alloys, which prove the homogeneously distributed irregular cuboidal precipitates are L_{12} -ordered structures. After 100 h aging at $800\text{ }^\circ\text{C}$, all three alloys are typical γ/γ' two-phase microstructures with cuboidal or coalesce cuboidal γ' (L_{12})-precipitates. The volume fraction of γ' precipitate in CVT-1 alloy is about 60%, while that in CVTW alloy is about 65%. CVTN alloy has the highest volume fraction of γ' precipitates of about 70%, suggesting that Nb is a stronger γ' former element than W. Compared to cast Nickel-based superalloys [48], the γ' precipitates in Co-V-Ti-based alloys have a more cubic morphology but unlike the irregular shaped precipitates in Co-12Ti alloy [29]. W addition significantly decreases the size of γ' (L_{12})-precipitates while the size of γ' phase is slightly increased by addition of Nb. The cube edge lengths of γ' (L_{12})-precipitates in CVT-1 and CVTN (Figure 2a,b) are about 130 nm and 160 nm, respectively, while the CVTW (Figure 2c) alloy has the smallest size of about 100 nm.

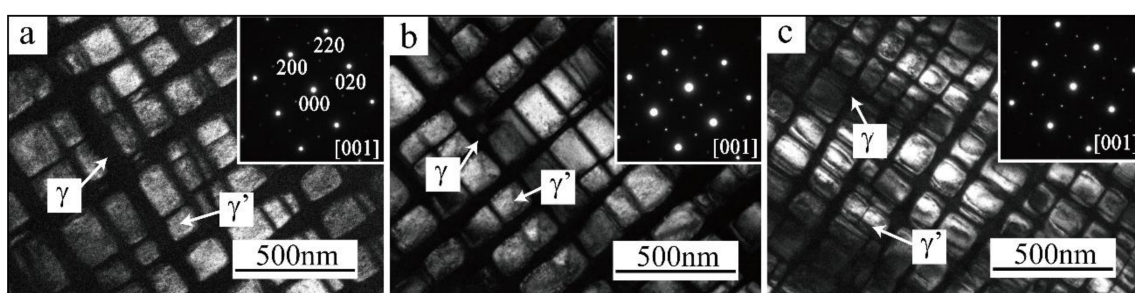


Figure 2. TEM dark-field images (DFI) obtained from the alloys annealed at $800\text{ }^\circ\text{C}$ for 100 h: (a) CVT-1; (b) CVTN; and (c) CVTW.

The partitioning behavior of different elements across the γ matrix and γ' precipitate was studied through elemental mapping using a STEM nanoprobe (FEI, Hillsboro, OR, USA). Figure 3 shows the elemental mapping results, which indicate vanadium, titanium, niobium, and tungsten primarily partition to the L_{12} -ordered precipitates. The elemental partitioning coefficients could influence the stabilities of γ' (L_{12})-precipitates and mechanical properties in Nickel-based superalloys [1,49]. The partitioning coefficient K_X is described as $K_X = C_{\gamma'}/C_{\gamma}$ ($C_{\gamma'}$ and C_{γ} are the concentration of element X in γ' and γ phases). The partition coefficient $K_X > 1$ indicates element X tends to

partition into γ' , while tends to distribute into γ when $K_X < 1$. Semiquantitative analyses of the partition behavior of alloys, which were aged at 800 °C for 100 h, were carried out by TEM equipped with energy-dispersive X-ray spectroscopy (EDS) detector (FEI, Hillsboro, OR, USA). The results are listed in Table 2. The compositions of γ were measured as Co-10.9V-2.3Ti, Co-8.2V-2.5Ti-1.3Nb and Co-7.9V-3.3Ti-1.9W (at. %), while the compositions of γ' were measured as Co-15.6V-7.2Ti, Co-14.3V-6.2Ti-2.7Nb and Co-13.2V-6.9Ti-2.1W (at. %). Both Nb and W are proven to be strong γ' -former elements in Co-V-Ti-based superalloys ($K_{Nb} = 2.07$, $K_W = 1.10$); while having a stronger γ' increases the strength, having a weaker γ' decreases it. This indicates that phase stabilities and mechanical properties of Co-V-Ti-based superalloys might be improved by additions of Nb and W.

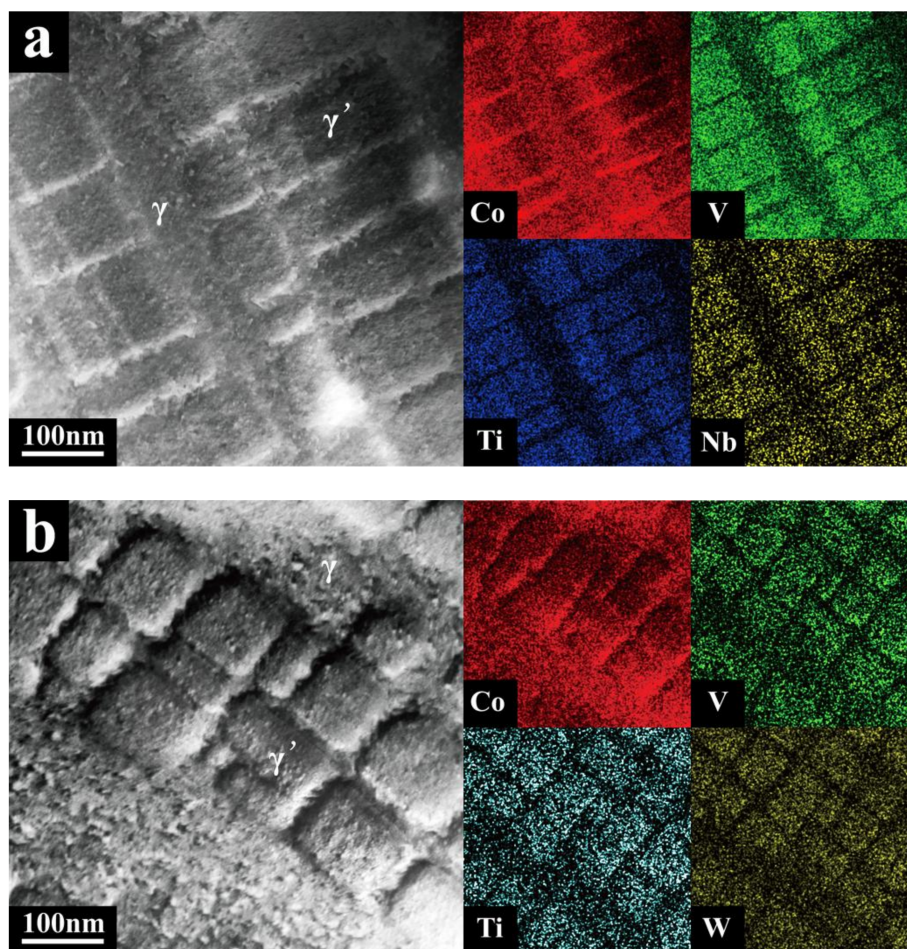


Figure 3. STEM HAADF image in the [001] zone axis and elemental mapping for the cuboidal precipitates using a STEM nanoprobe: (a) CVTN; and (b) CVTW.

Table 2. Compositions of the γ and γ' phases in present alloys.

Alloy Designation	Compositions (at. %)	
	γ	γ'
CVT-1	Co-10.9V-2.3Ti	Co-15.6V-7.2Ti
CVTN	Co-8.2V-2.5Ti-1.3Nb	Co-14.3V-6.2Ti-2.7Nb
CVTW	Co-7.9V-3.3Ti-1.9W	Co-13.2V-6.9Ti-2.1W

The SEM images using secondary electron mode of γ' ($L1_2$)-precipitates in long-time aging alloys are displayed in Figure 4a–c. No third-phases are found in grain boundaries of CVT-1, CVTN and CVTW alloys after 720 h of aging at 800 °C, as shown in Figure 3. The γ' precipitates of all experimental

alloys remain cuboidal or coalesce cuboidal without rafting after 720 h aging, indicating these are stable at 800 °C. Aging for a long time significantly increased the size of γ' (L_{12})-precipitates in all experimental alloys, indicating that coagulation and coalescence mechanisms occur among about cuboids after 720 h of aging treatment. The same effects of aging time in Nickel-based superalloy Ni-Al-Cr-W [8] and Co-Al-W-based [50,51] superalloys have been reported. After 720 h of aging, the size of γ' (L_{12})-precipitates of CVT-1 is about 220 nm and CVTW is about 170 nm compared to 130 nm and 100 nm, respectively. Significant coarsening in Nb-containing alloy occurred after 720 h aging; the CVTN alloy shows the largest size of γ' (L_{12})-precipitates which is about 280 nm. Nb is found to accelerate the growth of γ' phase. W addition can slow down the γ' phase from coarsening and significantly refine size of γ' phase. Of the data gathered, W-containing alloy remains small cuboid after 720 h aging without significant coarsening, because W is proven to be the slowest diffusing element among Nb, W and V in fcc Co while the diffusion velocity of Nb is the fastest [52]. Figure 4a–c shows that additions of Nb and W raise the volume fractions of γ' (L_{12})-precipitates with respect to the alloy CVT-1. The volume fractions of γ' (L_{12})-precipitates of all experimental alloys after 720 h aging are almost unchanging compared to that aging of 100 h.

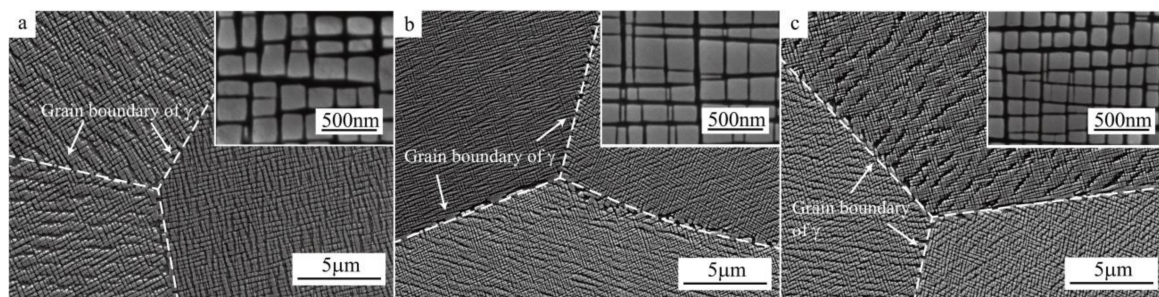


Figure 4. SEM images obtained from the alloys annealed at 800 °C for 720 h: (a) CVT-1; (b) CVTN; and (c) CVTW.

3.2. Phase Stability

The dissolution temperature of γ' precipitate in γ matrix is an indicator of phase stability of γ' phase. Currently, the additions of refractory alloying elements have been reported to increase the γ' solvus temperatures of Co-Al-W-based superalloys [20,21]. Nb has always been considered as a strong γ' former element, and it can significantly improve the stabilities of γ' in superalloys. The elemental partitioning coefficient of Nb in Co-V-Ti-based superalloys exceeds 2 (Table 2), indicating higher γ' solvus temperature. It is reported that the γ' solvus temperatures of Co-Al-W-based alloys would increase with the increasing of W content [46,47].

Figure 5 shows the influence of Nb and W to Co-V-Ti-based alloys on γ' solvus temperatures and melting temperatures as determined through heating experiment in the DSC. As a comparison, the phase transition points of Co-9Al-9W alloy [7], commercial Nickel-based superalloys Waspaloy [53] and IN939 [54] are also provided (Table 3). The γ' solvus temperature of CVT-1 alloy has a value of about 1023 °C, which is slightly increased by an addition of W. The γ' solvus temperature of CVTW alloy is about 1035 °C, which is 35 °C higher than Co-9Al-9W alloy (1000 °C) and completely comparable with Waspaloy (1030 °C). The addition of Nb has significantly increased the γ' solvus temperature, and CVTN has the highest γ' solvus temperature of about 1055 °C among all examined alloys in this investigation, which is about 55 °C higher than Co-9Al-9W alloy (1000 °C) and about 25 °C higher than Waspaloy (1030 °C). The melting temperature of CVTN is about 1254 °C that is about 100 °C higher than IN939 (1150 °C). The CVTW shows the highest melting temperature of about 1313 °C, which is about 160 °C higher than IN939 (1150 °C) and comparable with Waspaloy (1329 °C). Nb and W additions have significantly stabilized the γ' precipitates and increased the γ' solvus temperatures.

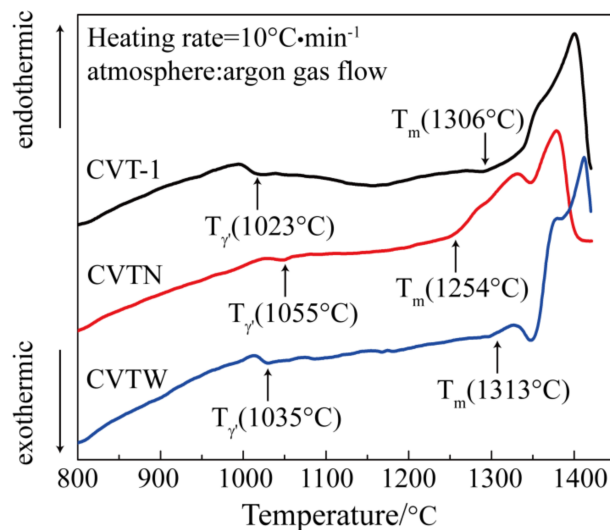


Figure 5. DSC heating curves obtained from: (a) CVT-1; (b) CVTN; and (c) CVTW.

Table 3. Phase transition temperatures and mass densities of alloys of present investigation as well as commercially available cobalt-based and nickel-based superalloys.

Alloy Designation	γ' Solvus Temperature (°C)	Melting Temperature (°C)	Mass Densities ($\text{g}\cdot\text{cm}^{-3}$)
CVT-1	1023	1306	8.23
CVTN	1055	1254	8.31
CVTW	1035	1313	8.50
Co-9Al-9W [7,38]	1000	1450	9.80
Waspaloy [48,53]	1030	1329	8.21
IN939 [48,54]	1100	1150	8.20
MarM509 [48]	-	1330	8.85

3.3. Mass Densities and Mechanical Properties

The Vickers-hardnesses of CVT-1, CVTN and CVTW were measured to be about 408 HV9.8, 448 HV9.8 and 482 HV9.8 at room temperature, respectively, which are higher than Co-9Al-9W (~400) [7] and Waspaloy (~390) [7]. Figure 6a shows plots of 0.2% flow stress versus temperature for alloy CVT-1, CVTN and CVTW. For bench-marking, the high temperature strengths of commercial Nickel-based superalloys (Waspaloy [53] and IN939 [6]), conventional Cobalt-based superalloy (MarM509 [48]) and Cobalt-based superalloy strengthened by γ' (L1₂)-precipitates (Co-9Al-9W [7]) are also included. The 0.2% flow stresses of all examined alloys are higher than MarM509 [48] and Co-9Al-9W [7] in all tested temperatures.

The room temperature 0.2% flow stress of CVT-1 is about 750 MPa, and significantly increased by additions of Nb and W. CVTN and CVTW show attractive room temperature strengths of about 860 MPa and 890 MPa, which are higher than all 0.2% flow stresses of alloys for comparison. The strengths of CVT-1, CVTN and CVTW decrease rapidly with increasing temperature, showing minimums of about 468 MPa, 504 MPa and 567 MPa at 600 °C, respectively.

When temperature exceeds 600 °C, 0.2% flow stresses of CVT-1, CVTN and CVTW increase rather than decrease with rising temperature. The anomalous positive temperature dependence of flow stress has also reported in Co-Al-W-based superalloys [17] and some of the Nickel-based superalloys containing γ' (L1₂) ordered precipitates in the fcc matrix [55,56], indicating that might favor their high temperature utilizations. Because of elastic anisotropy and lower anti-phase boundary (APB) energy on {001} planes, the activation of multiple slip modes at high temperature within γ' (L1₂) ordered precipitates, which lock cross-slipped 1/2<110> dislocations from the {111} octahedral planes to {100} cube planes, causes the abnormal phenomenon [57]. The peak temperature of alloy CVT-1 is 750 °C,

and the flow stress is about 523 MPa. Addition of W reduces the peak temperature of CVT-1 by 50 °C. The peak temperature of CVTW alloy is the same as Co-9Al-9W, locating at 700 °C, and the flow stress reaches about 588 MPa, which is much higher than Co-9Al-9W (480 MPa). The peak temperature of alloy CVTN is 50 °C higher than Co-9Al-9W and the flow stress is about 638 MPa, which is even comparable with commercial Nickel-based superalloy IN939 (632 MPa) at 750 °C due to the large flow stress anomalies.

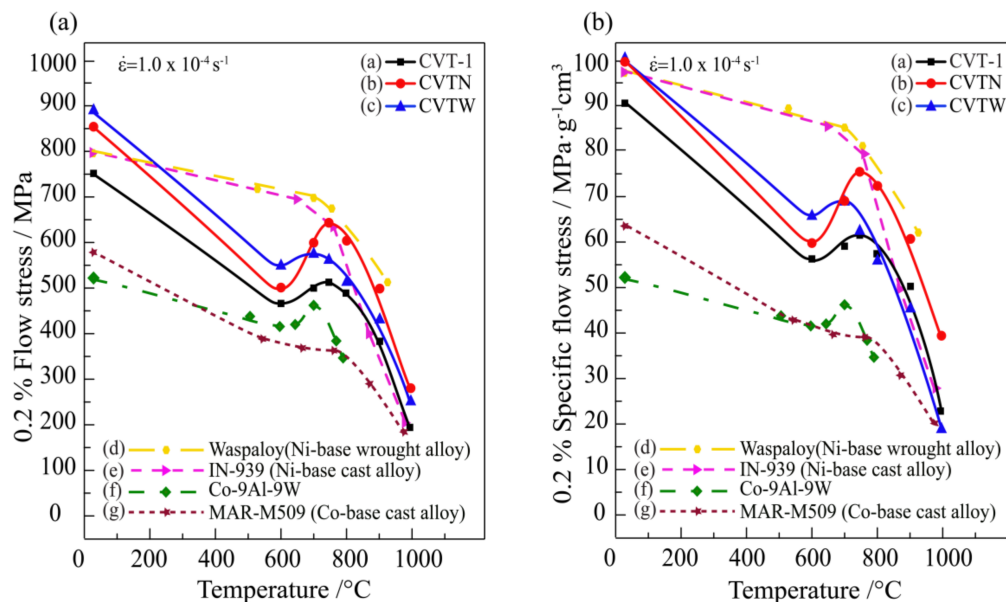


Figure 6. (a) Comparison of the 0.2% specific flow stress versus temperature curves of CVT-1, CVTN, CVTW, Co-9Al-9W (data from [7]), Waspaloy (data from [53]), IN939 (data from [6]) and MarM509 (data from [48]). (b) Comparison of the 0.2% specific flow stress versus temperature curves of CVT-1, CVTN, CVTW, Co-9Al-9W (data from [7]), Waspaloy (data from [53]), IN939 (data from [6]) and MarM509 (data from [48]).

The 0.2% flow stresses of both examined alloys exhibit negative temperature dependence again above their peak temperatures. The explanations of this phenomenon above peak temperature are controversial. It is widely accepted as one of the explanations that slip on the cube plane is activated [3]. Slip on octahedral plane above the peak temperature was observed by Suzuki et al. [13,16,17], who investigated deformation behavior of Co-Al-W-based superalloys. Moreover, the interaction mechanism between $1/3\langle 112 \rangle$ partial dislocations and γ' particles transforms from shearing to bypassing with increasing temperature, which, combined with activation of the slip on cube plane, might lead to rapid decrease of the 0.2% flow stresses of present studied alloys above peak temperatures. The strength curve of CVTN surpasses that of IN939 again above 750 °C, making alloy CVTN a promising material for use at higher temperature.

The mass densities of experimental alloys compared with commercial Nickel-based superalloys and other Cobalt-based superalloys are shown in Table 3. The densities of CVTN and CVTW alloys were measured to be $8.31 \text{ g} \cdot \text{cm}^{-3}$ and $8.50 \text{ g} \cdot \text{cm}^{-3}$, respectively, which are much lower than existing Cobalt-based superalloys. It is worth mentioning that the mass density of alloy CVTN is even comparable to commercial Nickel-based superalloys. The 0.2% specific flow stresses for experimental alloys and alloys for comparison are plotted as a function of temperature in Figure 6b. There are no significant changes after the 0.2% flow stresses normalized by the densities. The 0.2% specific flow stress of CVTW is about $69.2 \text{ MPa} / \text{g} \cdot \text{cm}^{-3}$ at 700 °C. CVTN exhibits great the 0.2% specific flow stress of about $76.9 \text{ MPa} / \text{g} \cdot \text{cm}^{-3}$ at 750 °C which is still comparable with IN939 ($77.1 \text{ MPa} / \text{g} \cdot \text{cm}^{-3}$),

although the density of IN-939 ($8.20 \text{ g}\cdot\text{cm}^{-3}$) is slightly lower than CVTN ($8.31 \text{ g}\cdot\text{cm}^{-3}$), indicating that Co-V-Ti-based superalloys might be helpful in further reducing mass densities of superalloys.

4. Conclusions

The microstructures, elemental partition behavior, phase stabilities, and mechanical properties of quaternary γ/γ' two phase Co-V-Ti-X (X: Nb, W) superalloys were investigated. The compositions of γ were measured as Co-8.2V-2.5Ti-1.3Nb and Co-7.9V-3.3Ti-1.9W (at. %), while the compositions of γ' were measured as Co-14.3V-6.2Ti-2.7Nb and Co-13.2V-6.9Ti-2.1W (at. %) in CVTN and CVTW, respectively. As a result, both Nb and W are proven to be γ' -former elements in Co-V-Ti-based superalloys and the partition coefficient of Nb is 2.07 while that of W is 1.10. The addition of Nb increases the γ' solvus temperature of Co-V-Ti-based superalloys from 1023 °C to 1055 °C, while that of W-containing alloy is only 1035 °C. The volume fraction of γ' precipitates in alloy CVT-1 is about 60%, and that in alloy CVTW is about 65%. CVTN alloy has the highest volume fraction of γ' precipitates of about 70%. This indicates that Nb is a stronger γ' -former element than W. The γ' volume fractions and γ' solvus temperatures of Co-V-Ti-based superalloys have been significantly increased by alloying with Nb. Moreover, the addition of Nb can also improve the mechanical properties of Co-V-Ti-based superalloys. Nb addition has increased the maximum flow stress of Co-V-Ti-based superalloys from 523 MPa to 638 MPa, making it comparable with commercial Nickel-based superalloy IN939 when temperature exceeds 750 °C. These features make CVTN alloy attractive for high-temperature applications.

Author Contributions: Conceptualization, X.L. and C.W.; Formal Analysis, Y.P. and Y.C.; Investigation, Y.P., Y.L. and Y.Y.; Writing—Original Draft Preparation, Y.P.; Writing—Review and Editing, Y.P., S.Y., J.R. and J.H.; Visualization, Y.P.; Supervision, X.L. and C.W.; and Funding Acquisition, X.L. and C.W.

Funding: This research was funded by the National Key R&D Program of China (Grant No. 2017YFB0702901) and the Ministry of Science and Technology of China (Grant No. 2014DFA53040).

Acknowledgments: This work was supported by the National Key R&D Program of China (Grant No. 2017YFB0702901) and the Ministry of Science and Technology of China (Grant No. 2014DFA53040).

Conflicts of Interest: The authors declare no conflict of interest.

References

1. Koizumi, Y.; Kobayashi, T.; Yokokawa, T.; Zhang, J.X.; Osawa, M.; Harada, H.; Aoki, Y.; Arai, M. Development of next-generation Ni-base single crystal superalloys. *J. Jpn. Inst. Metals* **2004**, *67*, 35–43.
2. Pollock, T.M.; Tin, S. Nickel-based superalloys for advanced turbine engines: Chemistry, microstructure and properties. *J. Propuls. Power* **2006**, *22*, 361–374. [[CrossRef](#)]
3. Reed, R.C. *The Superalloys: Fundamentals and Applications*; Cambridge University Press: Cambridge, UK, 2006; pp. 1–4. ISBN 978-05-2107-011-9.
4. Reed, R.C.; Tao, T.; Warnken, N. Alloys-by-design: Application to nickel-based single crystal superalloys. *Acta Mater.* **2009**, *57*, 5898–5913. [[CrossRef](#)]
5. Pollock, T.M. Alloy design for aircraft engines. *Nat. Mater.* **2016**, *15*, 809–815. [[CrossRef](#)] [[PubMed](#)]
6. Sims, C.T.; Stoloff, N.S.; Hagel, W.C. *Superalloys ii*; Materialsence: Eindhoven, The Netherlands, 1987; pp. 580–585. ISBN 978-04-7101-147-7.
7. Sato, J.; Omori, T.; Oikawa, K.; Ohnuma, I.; Kainuma, R.; Ishida, K. Cobalt-base high-temperature alloys. *Science* **2006**, *312*, 90–91. [[CrossRef](#)] [[PubMed](#)]
8. Neumeier, S.; Rehman, H.U.; Neuner, J.; Zenk, C.H.; Michel, S.; Schuwalow, S.; Rogal, J.; Drautz, R.; Göken, M. Diffusion of solutes in fcc cobalt investigated by diffusion couples and first principles kinetic monte carlo. *Acta Mater.* **2016**, *106*, 304–312. [[CrossRef](#)]
9. Samuel, L.C. *Precipitation-Hardening Characteristics of Ternary Cobalt-Aluminum-X Alloys*; The University of Arizona: Tucson, Arizona, 1971.
10. Pollock, T.M.; Dibbern, J.; Tsunekane, M.; Zhu, J.; Suzuki, A. New Co-based γ - γ' high-temperature alloys. *JOM* **2010**, *62*, 58–63. [[CrossRef](#)]

11. Yan, H.Y.; Vorontsov, V.A.; Coakley, J.; Jones, N.G.; Stone, H.J.; Dye, D. Quaternary alloying effects and the prospects for a new generation of Co-base superalloys. In *Superalloys*; John Wiley & Sons: Hoboken, NJ, USA, 2012; pp. 705–714.
12. Tanaka, K.; Inui, H. Effects of alloying elements on physical and mechanical properties of Co-Al-W-based L1₂/fcc two-phase alloys. *Mater. Sci. Forum* **2014**, *783–786*, 1195–1200. [[CrossRef](#)]
13. Suzuki, A.; Inui, H.; Pollock, T.M. L1₂-strengthened cobalt-base superalloys. *Annu. Rev. Mater. Res.* **2015**, *45*, 345–368. [[CrossRef](#)]
14. Chinen, H.; Sato, J.; Omori, T.; Oikawa, K.; Ohnuma, I.; Kainuma, R.; Ishida, K. New ternary compound Co₃(Ge, W) with L1₂ structure. *Scr. Mater.* **2007**, *56*, 141–143. [[CrossRef](#)]
15. Chinen, H.; Omori, T.; Oikawa, K.; Ohnuma, I.; Kainuma, R.; Ishida, K. Phase equilibria and ternary intermetallic compound with L1₂ structure in Co-W-Ga system. *J Phase Equilib. Diffus.* **2009**, *30*, 587–594. [[CrossRef](#)]
16. Suzuki, A.; DeNolf, G.C.; Pollock, T.M. Flow stress anomalies in γ/γ' two-phase Co–Al–W-base alloys. *Scr. Mater.* **2007**, *56*, 385–388. [[CrossRef](#)]
17. Suzuki, A. High-temperature strength and deformation of γ/γ' two-phase Co–Al–W-base alloys. *Acta Mater.* **2008**, *56*, 1288–1297. [[CrossRef](#)]
18. Shinagawa, K.; Omori, T.; Sato, J.; Oikawa, K.; Ohnuma, I.; Kainuma, R.; Ishida, K. Phase equilibria and microstructure on γ' phase in Co-Ni-Al-W system. *Mater. Trans.* **2008**, *49*, 1474–1479. [[CrossRef](#)]
19. Shinagawa, K.; Omori, T.; Oikawa, K.; Kainuma, R.; Ishida, K. Ductility enhancement by boron addition in Co–Al–W high-temperature alloys. *Scr. Mater.* **2009**, *61*, 612–615. [[CrossRef](#)]
20. Bauer, A.; Neumeier, S.; Pyczak, F.; Göken, M. Microstructure and creep strength of different γ/γ' -strengthened Co-base superalloy variants. *Scr. Mater.* **2010**, *63*, 1197–1200. [[CrossRef](#)]
21. Ooshima, M.; Tanaka, K.; Okamoto, N.L.; Kishida, K.; Inui, H. Effects of quaternary alloying elements on the γ' solvus temperature of Co–Al–W based alloys with fcc/L1₂ two-phase microstructures. *J. Alloys Compd.* **2010**, *508*, 71–78. [[CrossRef](#)]
22. Kobayashi, S.; Tsukamoto, Y.; Takasugi, T. The effects of alloying elements (Ta, Hf) on the thermodynamic stability of γ' -Co₃(Al, W) phase. *Intermetallics* **2012**, *31*, 94–98. [[CrossRef](#)]
23. Omori, T.; Oikawa, K.; Sato, J.; Ohnuma, I.; Kattner, U.R.; Kainuma, R.; Ishida, K. Partition behavior of alloying elements and phase transformation temperatures in Co–Al–W-base quaternary systems. *Intermetallics* **2013**, *32*, 274–283. [[CrossRef](#)]
24. Titus, M.S.; Suzuki, A.; Pollock, T.M. Creep and directional coarsening in single crystals of new γ - γ' cobalt-base alloys. *Scr. Mater.* **2012**, *66*, 574–577. [[CrossRef](#)]
25. Eggeler, Y.M.; Titus, M.S.; Suzuki, A.; Pollock, T.M. Creep deformation-induced antiphase boundaries in L1₂-containing single-crystal cobalt-base superalloys. *Acta Mater.* **2014**, *77*, 352–359. [[CrossRef](#)]
26. Shi, L.; Yu, J.J.; Cui, C.Y.; Sun, X.F. The creep deformation behavior of a single-crystal Co–Al–W-base superalloy at 900 °C. *Mater. Sci. Eng. A* **2015**, *635*, 50–58. [[CrossRef](#)]
27. Bauer, A.; Neumeier, S.; Pyczak, F.; Göken, M. *Creep Strength and Microstructure of Polycrystalline γ' -Strengthened Cobalt-Base Superalloys*; John Wiley & Sons, Inc.: Hoboken, NJ, USA, 2012; pp. 695–703.
28. Pyczak, F.; Bauer, A.; Göken, M.; Neumeier, S.; Lorenz, U.; Oehring, M.; Schell, N.; Schreyer, A.; Stark, A.; Symanzik, F. Plastic deformation mechanisms in a crept L1₂ hardened Co-base superalloy. *Mater. Sci. Eng. A* **2013**, *571*, 13–18. [[CrossRef](#)]
29. Zenk, C.H.; Neumeier, S.; Stone, H.J.; Göken, M. Mechanical properties and lattice misfit of γ/γ' strengthened Co-base superalloys in the Co–W–Al–Ti quaternary system. *Intermetallics* **2014**, *55*, 28–39. [[CrossRef](#)]
30. Titus, M.S.; Mottura, A.; Babu Viswanathan, G.; Suzuki, A.; Mills, M.J.; Pollock, T.M. High resolution energy dispersive spectroscopy mapping of planar defects in L1₂-containing Co-base superalloys. *Acta Mater.* **2015**, *89*, 423–437. [[CrossRef](#)]
31. Titus, M.S.; Eggeler, Y.M.; Suzuki, A.; Pollock, T.M. Creep-induced planar defects in L1₂-containing Co- and CoNi-base single-crystal superalloys. *Acta Mater.* **2015**, *82*, 530–539. [[CrossRef](#)]
32. Meher, S.; Yan, H.Y.; Nag, S.; Dye, D.; Banerjee, R. Solute partitioning and site preference in γ/γ' cobalt-base alloys. *Scr. Mater.* **2012**, *67*, 850–853. [[CrossRef](#)]
33. Bocchini, P.J.; Lass, E.A.; Moon, K.-W.; Williams, M.E.; Campbell, C.E.; Kattner, U.R.; Dunand, D.C.; Seidman, D.N. Atom-probe tomographic study of γ/γ' interfaces and compositions in an aged Co–Al–W superalloy. *Scr. Mater.* **2013**, *68*, 563–566. [[CrossRef](#)]

34. Meher, S.; Banerjee, R. Partitioning and site occupancy of ta and mo in Co-base γ/γ' alloys studied by atom probe tomography. *Intermetallics* **2014**, *49*, 138–142. [[CrossRef](#)]
35. Povstugar, I.; Choi, P.-P.; Neumeier, S.; Bauer, A.; Zenk, C.H.; Göken, M.; Raabe, D. Elemental partitioning and mechanical properties of Ti- and ta-containing Co–Al–W-base superalloys studied by atom probe tomography and nanoindentation. *Acta Mater.* **2014**, *78*, 78–85. [[CrossRef](#)]
36. Mughrabi, H. The importance of sign and magnitude of γ/γ' lattice misfit in superalloys—With special reference to the new γ' -hardened cobalt-base superalloys. *Acta Mater.* **2014**, *81*, 21–29. [[CrossRef](#)]
37. Yan, H.Y.; Vorontsov, V.A.; Dye, D. Alloying effects in polycrystalline γ' strengthened Co–Al–W base alloys. *Intermetallics* **2014**, *48*, 44–53. [[CrossRef](#)]
38. Makineni, S.K.; Nithin, B.; Chattopadhyay, K. Synthesis of a new tungsten-free γ - γ' cobalt-based superalloy by tuning alloying additions. *Acta Mater.* **2015**, *85*, 85–94. [[CrossRef](#)]
39. Makineni, S.K.; Nithin, B.; Chattopadhyay, K. A new tungsten-free γ - γ' Co–Al–Mo–Nb-based superalloy. *Scr. Mater.* **2015**, *98*, 36–39. [[CrossRef](#)]
40. Lass, E.A.; Williams, M.E.; Campbell, C.E.; Moon, K.-W.; Kattner, U.R. γ' phase stability and phase equilibrium in ternary Co–Al–W at 900 °C. *J. Phase Equilib. Diffus.* **2014**, *35*, 711–723. [[CrossRef](#)]
41. Wee, D.M.; Noguchi, O.; Oya, Y.; Suzuki, T. New L1₂ ordered alloys having the positive temperature dependence of strength. *Trans. Jpn. Inst. Metals* **2007**, *21*, 237–247. [[CrossRef](#)]
42. Zenk, C.H.; Povstugar, I.; Li, R.; Rinaldi, F.; Neumeier, S.; Raabe, D.; Göken, M. A novel type of Co–Ti–Cr-base γ/γ' superalloys with low mass density. *Acta Mater.* **2017**, *135*, 244–251. [[CrossRef](#)]
43. Ruan, J.J.; Wang, C.P.; Zhao, C.C.; Yang, S.Y.; Yang, T.; Liu, X.J. Experimental investigation of phase equilibria and microstructure in the Co–Ti–V ternary system. *Intermetallics* **2014**, *49*, 121–131. [[CrossRef](#)]
44. Liu, Y.; Takasugi, T.; Izumi, O.; Suenaga, H. Mechanical properties of Co₃Ti polycrystals alloyed with various additions. *J. Mater. Sci.* **1989**, *24*, 4458–4466. [[CrossRef](#)]
45. Ruan, J.J.; Liu, X.J.; Yang, S.Y.; Xu, W.W.; Omori, T.; Yang, T.; Deng, B.; Jiang, H.X.; Wang, C.P.; Kainuma, R.; et al. Novel Co–Ti–V-base superalloys reinforced by L1₂-ordered γ' phase. *Intermetallics* **2018**, *92*, 126–132. [[CrossRef](#)]
46. Bocchini, P.J.; Sudbrack, C.K.; Sauza, D.J.; Noebe, R.D.; Seidman, D.N.; Dunand, D.C. Effect of tungsten concentration on microstructures of Co-10Ni-6Al-(0,2,4,6)W-6Ti (at%) cobalt-based superalloys. *Mater. Sci. Eng. A* **2017**, *700*, 481–486. [[CrossRef](#)]
47. Pyczak, F.; Bauer, A.; Göken, M.; Lorenz, U.; Neumeier, S.; Oehring, M.; Paul, J.; Schell, N.; Schreyer, A.; Stark, A.; et al. The effect of tungsten content on the properties of L1₂-hardened Co–Al–W alloys. *J. Alloys Compd.* **2015**, *632*, 110–115. [[CrossRef](#)]
48. Davis, J.R. *ASM Specialty Handbook: Nickel, Cobalt, and Their Alloys*; John Wiley & Sons: Hoboken, NJ, USA, 2000; pp. 345–370. ISBN 0-87170-685-7.
49. Zhang, J.X.; Murakumo, T.; Harada, H.; Koizumi, Y.; Kobayashi, T. Creep deformation mechanisms in some modern single-crystal superalloys. In *Superalloys*; John Wiley & Sons: Hoboken, NJ, USA, 2004; pp. 189–195.
50. Sauza, D.J.; Bocchini, P.J.; Dunand, D.C.; Seidman, D.N. Influence of ruthenium on microstructural evolution in a model Co Al W superalloy. *Acta Mater.* **2016**, *117*, 135–145. [[CrossRef](#)]
51. Zhou, H.J.; Xue, F.; Chang, H.; Feng, Q. Effect of mo on microstructural characteristics and coarsening kinetics of γ' precipitates in Co–Al–W–Ta–Ti alloys. *J. Mater. Sci. Technol.* **2018**, *34*, 799–805. [[CrossRef](#)]
52. Sudbrack, C.K.; Ziebell, T.D.; Noebe, R.D.; Seidman, D.N. Effects of a tungsten addition on the morphological evolution, spatial correlations and temporal evolution of a model Ni–Al–Cr superalloy. *Acta Mater.* **2008**, *56*, 448–463. [[CrossRef](#)]
53. Committee, A.I.H.; Davis, J.R.; Abel, L.A. Properties and Selection: Irons, Steels, and High-Performance Alloys. In *Metals Handbook*; CRC Press: Boca Raton, FL, USA, 1990; pp. 2287–2371. ISBN 0-87170-377-7.
54. Jahangiri, M.R.; Boutorabi, S.M.A.; Arabi, H. Study on incipient melting in cast Ni base In939 superalloy during solution annealing and its effect on hot workability. *Mater. Sci. Technol.* **2013**, *28*, 1402–1413. [[CrossRef](#)]
55. Paidar, V.; Pope, D.P.; Vitek, V. A theory of the anomalous yield behavior in L1₂ ordered alloys. *Acta Metall.* **1984**, *32*, 435–448. [[CrossRef](#)]

56. Hirsch, P.B. A model of the anomalous yield stress for (111) slip in $L1_2$ alloys. *Prog. Mater. Sci.* **1992**, *36*, 63–88. [[CrossRef](#)]
57. Takeuchi, S.; Kuramoto, E. Temperature and orientation dependence of the yield stress in Ni_3Ga single crystals. *Acta Metall.* **1973**, *21*, 415–425. [[CrossRef](#)]



© 2018 by the authors. Licensee MDPI, Basel, Switzerland. This article is an open access article distributed under the terms and conditions of the Creative Commons Attribution (CC BY) license (<http://creativecommons.org/licenses/by/4.0/>).